# Numerical Evaluation of Flow Conditions in the LENS Reflected Shock-Tunnel Facilities

Matthew MacLean*
*Calspan-UB Research Center (Buffalo, NY 14225)*

Graham Candler†
*University of Minnesota (Minneapolis, MN)*

*and*

Michael Holden‡
*Calspan-UB Research Center (Buffalo, NY 14225)*

**The calculation process of the flowfield of the nozzles of the Calspan-UB Research Center reflected shock tunnel facilities has been described. These calculations utilize a full Navier-Stokes solver based on the robust data-parallel line relaxation method coupled with chemical and vibrational non-equilibrium effects as well as the inclusion of a non-ideal equation of state necessitated by the high pressures in the reservoir of the shock tunnel. The calculation of the reservoir conditions and the modeling of the turbulent boundary layer in the throat region have been found to be the two most significant issues associated with the computation. With the use of the Spalart-Allmaras one-equation model, the error calculated by comparing the solution to measured Pitot pressure profiles in the test section are nominally +/- 5% or less for all the cases considered. In addition to good agreement with the available experimental data, the calculations have proven to be important in the understanding of the flow interactions during the nozzle expansion and have provided a means of evaluating new nozzle throat inserts to generate new capability ranges for the facilities.**

## Nomenclature

| | | |
|---|---|---|
| $b_{0M}$ | = | non-ideal correction factor |
| $c$ | = | species mass fraction |
| $h$ | = | enthalpy |
| $M$ | = | Mach number |
| $P$ | = | pressure |
| $Q$ | = | dynamic pressure |
| R | = | species gas constant |
| $\tilde{R}$ | = | mixture effective gas constant |
| $Re$ | = | Reynolds number |
| $T$ | = | temperature |
| $T_V$ | = | vibrational temperature |
| $u$ | = | velocity (axial or 1D) |
| $W$ | = | incident shock speed |
| $W_R$ | = | reflected shock speed |
| $\rho$ | = | density |

*subscripts*

| | | |
|---|---|---|
| $i$ | = | summation index for chemical species |
| $k$ | = | summation index for iterations |
| $w$ | = | wall index |
| $0$ | = | reservoir or stagnation quantity |
| $1$ | = | state in driven tube |
| $2$ | = | post-incident shock state |
| $4$ | = | post-reflected (reservoir) state |
| $6$ | = | driver tube state |

* Senior Research Scientist, AIAA Member.
† Professor, AIAA Associate Fellow.
‡ AAEC Program Manager, AIAA Fellow.

## I. Introduction

THE shock tunnel is an experimental facility which is used for accurate aerothermal testing of vehicles at high Mach numbers. The stagnation enthalpy required to simulate flight conditions scales with Mach number squared, so, as flight Mach number increases, the required enthalpy becomes difficult to generate using conventional, steady-state-type facilities. For example, the stagnation or reservoir temperature of Mach 10 flight at an altitude of 30 km (98.5 kft) is nominally 5,000 K (9,000 $^{O}$R), a value which is above the feasible limit of most wind tunnel construction materials.

Failure to correctly duplicate this flight environment can have detrimental effects on the quality of a test program. Failure to duplicate the stagnation enthalpy of the flow in practice leads to a condition of a reduced velocity in the freestream flow of the facility. Flow features such as large-scale separation, shock/boundary-layer interactions, transitional and turbulent phenomena, and non-equilibrium chemistry effects – including combustion and mixing phenomena – may not be adequately represented in a low energy simulation. This can lead to inaccurate prediction of common design criteria such as heating levels, structural loading, control system dynamics, and overall vehicle performance.

Many schemes have been proposed to overcome this limitation and test at fully-duplicated (high enthalpy) conditions, therefore avoiding the problem of simulating the effects of such a flight with low energy tests and extrapolating to the flight condition. Among these schemes, the reflected shock tunnel is one of the most popular types of facilities used in the prediction of hypervelocity vehicle performance. The reflected shock tunnel uses a transient effect of an unsteady shock wave to heat a stagnant test gas to very high enthalpy levels for a short duration of time. This test gas may then be expanded through a converging-diverging nozzle in a manner similar to a blowdown facility to produce a hypervelocity test flow for a short duration. This process is described in more detail in Fig. 1.

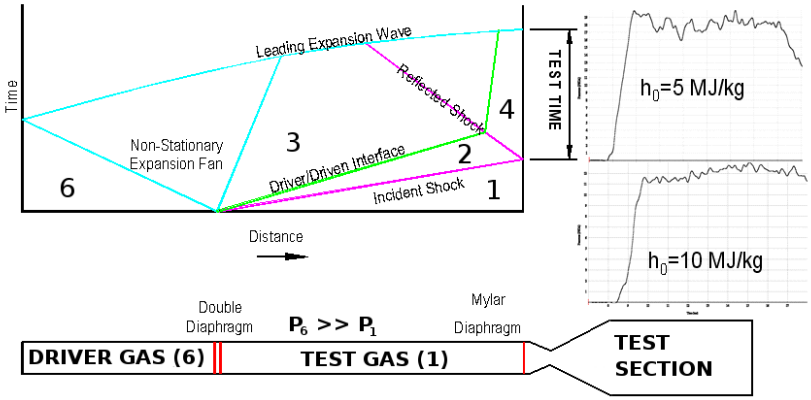


**Figure 1. Wave Diagram of a Typical Reflected Shock Tunnel Facility using Tailored Conditions.**

As demonstrated schematically in Fig. 1, a shocktube consists of a long tube composed of a high pressure driver gas and a low pressure test (driven) gas. A diaphragm or interface separates the two gases. At some initiation time, the diaphragm is suddenly removed, allowing the driver gas to expand into the driven tube. In the case of the LENS facilities, this effect is achieved using a double diaphragm apparatus with a small middle chamber. As shown on the wave diagram of Fig. 1, the unsteady expansion into the test gas produces a leading shock which serves to raise the temperature and pressure of the test gas. Because this moving shock must induce fluid motion behind it, a shock is reflected from the endwall of the shock tube back through the test gas, further raising the temperature and pressure. At this point, the test gas is at high pressure and high temperature and stagnant in the end of the shocktube. A nozzle may be placed at the end of the shocktube to expand this reservoir gas into the test area. Numerical details of equations governing shocktube operation are given by Anderson[1].

Test time of a reflected shock tunnel is governed by the time that it takes the driver gas to reach the endwall and contaminate the reservoir. If the shock tunnel is operated using “tailored” conditions, then the expansion of the driver gas is brought to a halt by the reflected shock wave, and test time is then limited by the first expansion wave that reaches the endwall. Tailored conditions always maximize the possible test time in a reflected shock tunnel, and the LENS facilities are always run as tailored facilities.

Testing in a reflected shock tunnel has many inherent difficulties associated with generating good quality conditions during an experiment. Many of these issues are mechanical in nature, such as creating a clean break of the diaphragm(s) between the shocktube sections, or designing an endwall diaphragm which will successfully reflect the incident shock but then disappear to allow for expansion of the reservoir gas into the nozzle and test sections.

Issues of this type will not be discussed here. This paper will focus on predicting the flow characteristics of the nozzle component of the LENS reflected shock tunnels. Because the flow of the nozzle is dependent on the operation of the shocktube components, some attention will be given to the tailored reservoir conditions that are produced in the shocktube as well.

## II. LENS Facility Overview

Hypervelocity testing at CUBRC utilizes several facilities. Currently, CUBRC operates the 48" reflected shock tunnel, LENS-I and LENS-II reflected shock tunnels[2], and the LENS-X expansion tunnel. An expansion tunnel is a modified shock tunnel that produces high enthalpy flows without the need to stagnate the test gas and thus introduce chemical dissociation contamination. The phenomena governing a test in an expansion tunnel are somewhat different than those in a reflected tunnel, so expansion tunnels will not be dealt with further here. One may see Nompelis, *et al.*[3] for an example of an expansion tunnel computation. Although each of the remaining three facilities has been designed to target a certain range of conditions, the operation of each tunnel is the same in principle.

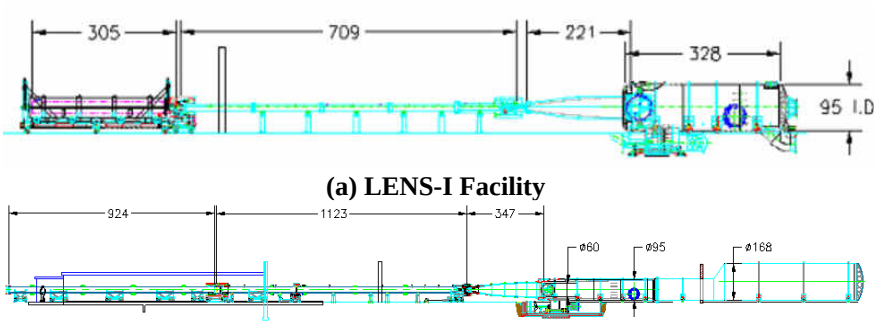


**(a) LENS-I Facility**

**(b) LENS-II Facility**

**Figure 2. Drawings of CUBRC LENS Hypervelocity Reflected Shock Tunnel Facilities with Nominal Dimensions [all values shown in inches].**

LENS-I was designed to be used for high-altitude, high Mach number testing. The facility is shown in Fig. 2a. Any mixture of $N_2$, He, and $H_2$ gases can be used as a driver gas to achieve tailoring for a given condition. The low molecular weight of the hydrogen driver gas allows the LENS-I facility to be tailored to produce freestream velocities of up to 4.3 km/s (14,000 ft/s). Driver pressure can be up to 600MPa (30,000 psia). The observed reservoir pressure during the steady-state test period in the shock tunnel will be some fractional recovery factor times this driver pressure (values like 80% are typical and are heavily dependent on conditions). For the driven, or test, gas, $N_2$, Air, and $CO_2$ have been used. The current compliment of nozzles covers a range from approximately Mach 7 to 18. The equivalent altitude in air that can be simulated in LENS-I ranges from 10 to 100 km (6 to 62 mi) depending on the Mach number and other conditions.

The LENS-II facility, shown in Fig. 2b, was designed for the low altitude, moderate Mach number testing of atmospheric interceptor vehicles. The facility is rated to produce conditions of Mach 4.5 at sea level dynamic pressure in the freestream, but it is the physical size of LENS-II which allows unparalleled testing capability. In total, the shocktube component is over 60 m (200 ft) long, allowing for as much as 100 ms of test time when operating the facility as a reflected shock tunnel. The test time is one to two orders of magnitude more than most other short-duration, pulse-type facilities. The size of LENS-II therefore provides enough time to perform dynamic event tests[4] at fully duplicated conditions without the large expense and high risk of flight testing. The shocktube is 61 cm (24 in) in diameter, with a 1.50 m (60 in) nozzle exit plane. Currently, nozzles exist for nominal Mach numbers of 3.5 through 7, while the facility could be extended as high as Mach 10. Driver gas mixtures of $N_2$ and/or He may be used in LENS-II, as hydrogen driver gas is not required to simulate the correct enthalpy levels at these Mach numbers.

The capability of the CUBRC facilities is summarized in Fig. 3, where a velocity-altitude map is shown with approximate bounds based on freestream flow conditions for each of the four facilities – LENS-I, LENS-II, LENS-X, and the 48" tunnel. This figure shows the capability range for air. Other test gases will have different ranges.

Understanding the flowfield of the nozzle and the freestream conditions observed at the model are an important part of the validation of the data obtained during an experiment in the LENS facilities. This fact has been particularly emphasized as CFD has become an increasingly integral part of these experimental programs. In most circumstances now, surface data from programs conducted in the LENS facilities are validated using computational predictions. These calculations are sensitive to the freestream conditions provided to the code. Incorrect freestream predictions will lead to discrepancies between prediction and experiment in surface heating and pressure levels,

creating the illusion of increased uncertainty or error in the experimental data collection measurements. CUBRC has also been heavily involved in code validation efforts for much of its history[5], an application where the accuracy of the freestream conditions is important to the improvement of numerical schemes and models[6].

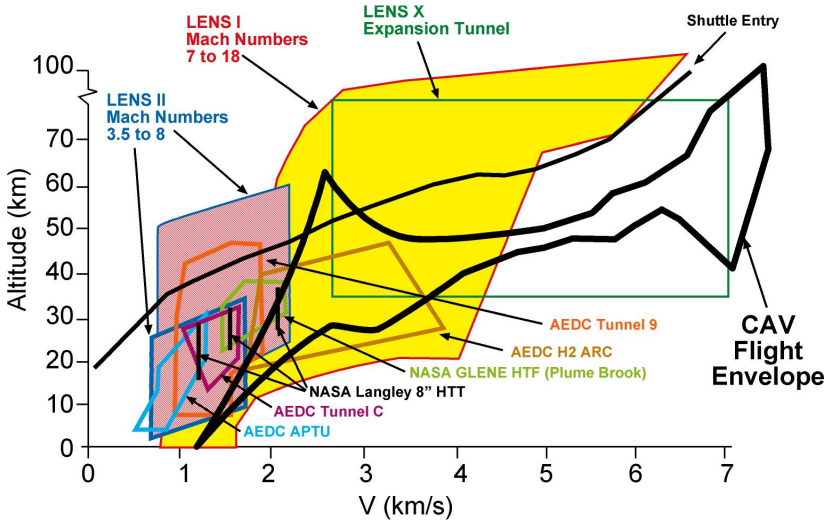


**Figure 3. Velocity-Altitude Map of the CUBRC Facilities using Air as a Test Gas**

The computation of nozzle flowfields begins with a discussion about computing the reservoir conditions of the nozzle. From Section I, the incident and reflected shocks shown in Fig. 1 create a high pressure, high temperature, stagnant region of gas which defines the reservoir conditions of the problem. The reservoir will have high enthalpy content, and will have a pressure equal to some fraction of the driver pressure that will be slightly less than one. If the tunnel can be well-tailored for the given condition, then this reservoir will be steady, indicating that few extraneous waves besides the two shocks influence the reservoir in end of the driven tube.

Several assumptions must be made for the following derivation. First, the steady run time of the tunnel should be sufficiently long that the nozzle has time to fully start, as it is driven by the steady reservoir conditions. The reservoir conditions should persist such that, at a minimum, the required amount of time elapses to set-up the steady flow phenomena on the model surface and to collect the data. This fact is important to support the assumption that the nozzle flow may be computed as a steady-state calculation. Failure to fulfill this criterion requires that the nozzle starting problem be treated in a transient manner, a calculation which is much more complex and prone to additional uncertainties. The physical size of the LENS tunnels justifies this assumption, as the nozzle starting process typically takes a very small amount of the total steady reservoir time.

The second assumption is that the reservoir is created by a single incident shock and a single reflected shock, such that there are no extraneous waves changing the reservoir flow conditions. This is the sign of correct tailoring of the tunnel flow conditions. Both LENS-I and LENS-II are typically well-tailored. Tailoring of the shocktube is facilitated by the fact that the LENS tunnels are well-described by one-dimensional characteristic theory because of their size, which minimizes viscous effects in the tube. This is tied to the third assumption – that the viscous effects in the shocktube will be small, so that the incident and reflected shock process will be governed by inviscid phenomena.

Again, the physical size and scale of the LENS facilities justifies all three of these assumptions. Smaller shock tunnels that may be dominated by viscous effects or which have very short steady run times that may be used up in starting the nozzle will have difficulty in justifying this set of assumptions. Such situations require solving a full transient (probably multi-dimensional) analysis, which increases overall uncertainty in the testing of the model. By making these assumptions in LENS, the problem of the nozzle flow may be reduced to the calculation of reservoir conditions based on simple normal shock relations in a moving coordinate system followed by a steady-state Navier Stokes analysis of the nozzle.

## III. Calculation of Shocktube Reservoir Conditions

The shocktube reservoir conditions may be estimated by considering a single, moving, normal shock. Upstream of this shock is designated state *#1*. Just after the shock passes through the fluid, we designate as state *#2a*. This incident shock then reflects off the endwall of the shocktube and a reflected shock moves back through the fluid in the other direction. Upstream of the reflected shock will be designated as state *#2b*, and finally downstream of the reflection (the reservoir state) we will call state *#4*. These states are also consistent with those labeled in Fig. 1.

The mass, momentum, and energy equations for the flow state across the incident shock are specified by eqns. (1), (2), and (3). These are the standard jump conditions across a one-dimensional discontinuity in the coordinate

system relative to the moving shock[7]. Some simplifications may be made by noticing that the states *2a* and *2b* are actually the same state, accounting for the change in coordinate system from *a* to *b*.

$$\rho_1 W = \rho_2 (W - u_2) \tag{1}$$

$$\rho_1 W^2 + P_1 = \rho_2 (W - u_2)^2 + P_2 \tag{2}$$

$$h_1 + \frac{1}{2} W = h_2 + \frac{1}{2} (W - u_2)^2 \tag{3}$$

Those same equations written for the discontinuity across the reflected shock are given by eqns. (4), (5), and (6).

$$\rho_2 (W_R + u_2) = \rho_4 W_R \tag{4}$$

$$\rho_2 (W_R + u_2)^2 + P_2 = \rho_4 W_R^2 + P_3 \tag{5}$$

$$h_2 + \frac{1}{2} (W_R + u_2)^2 = h_4 + \frac{1}{2} W_R^2 \tag{6}$$

In this situation, the state 1 is completely known. The pressure is a controlled pressure during the loading of the driven tube. The temperature is known to be the ambient temperature because the driven tube is allowed to equilibrate before the tunnel is run, so the density and enthalpy of state 1 can be calculated for a known gas composition. The incident shock speed, *W*, is measured using a series of high frequency *TOA* gages located uniformly down the length of the driven tube that respond to the passing of the shock. Also, a group of pressure transducers is placed in the endwall of the tunnel, so the reservoir pressure, $P_4$, is known during the shocktube event. Using these pieces of information, eqns. (1) – (6) may be solved for the six unknowns: $\rho_2$, $u_2$, $P_2$, $W_R$, $h_2$, and $h_4$. Here, the reservoir density, $\rho_4$ is obtained by including a suitable equation of state. These six equations may be used to eliminate all of the intermediate variables (which are unimportant to the desired outcome), and produce a single equation for reservoir enthalpy, $h_4$, in terms of the known variables. This relationship is given in eqn. (7).

$$h_4 = h_1 + \left[ W^2 + \frac{(P_4 - P_1)}{(\rho_4 - \rho_1)} \right] \left[ \frac{(P_4 - P_1)}{\rho_1 W^2 + \rho_4 \frac{(P_4 - P_1)}{(\rho_4 - \rho_1)}} \right] \tag{7}$$

This calculation thus far is straightforward, but the choice of equation of state requires further consideration. Large densities (often more than 100 kg/m$^3$) are often present in the reservoir state #4, so the ideal gas law does not strictly apply. Instead, we have used the excluded volume correction of Lordi and Mates[8] to account for these dense states. In the excluded volume approach, the ideal gas law is modified to exclude the volume occupied by the gas molecules at high density. This relation is given in eqn. (8).

$$P = \frac{\rho \tilde{R} T}{(1 - b_{0M} \rho)} \tag{8}$$

Here, the constant $b_{0M}$, called the co-volume, is a term involving the effective molecular diameter of the gas. The value is 0.00111996 $m^3/kg$ for air and nitrogen. One can see that for small to moderate densities, the ideal gas law is approximately returned, while the excluded volume effect becomes significant only for large densities. The enthalpy of the gas is also modified accordingly by the excluded volume equation.

The reservoir is calculated by assuming equilibrium dissociation of the gas. This is an important effect in air and $CO_2$, and the reservoir conditions in the LENS facilities can even cause some amount of nitrogen dissociation. Because of the large temperatures and densities of the reservoir, the relaxation times of the chemistry rates are very short. The standard equilibrium curve fits are used from Gordon and McBride[9], which are functions of temperature only. Diatomic species are also assumed to have relevant vibrational modes in full equilibrium with the translational temperature in the calculation of enthalpy. The details of the algorithm used to compute the reservoir conditions are listed in Fig. 4. This algorithm was found to be well-posed and convergent even with the included effects of equilibrium chemistry and the excluded volume, non-ideal gas law.

- Guess $\rho_4$
- Calculate $h_4$ from eqn. (7)
- Calculate $c_{i4}$ and $T_4$
  - Guess $T_4$
  - Compute equilibrium concentrations, $c_{i4}$
  - Compute $\tilde{R}(c_{i4})$
  - Compute $P^k$
  - If $P^k$ is not equal to $P_4$, then re-guess $T_4$
- Calculate $h^k$ ($T_4$, $c_{i4}$, $\rho_4$)
- If $h^k$ is not equal to $h_4$, then re-guess $\rho_4$.

**Figure 4. Flowchart of Algorithm for Computing Reservoir Conditions**

From Lordi and Mates, the non-ideal behavior of the test gas will affect its compressibility on the order of 1% at ten times sea level density and on the order of 10% for one-hundred times sea level density. In the reservoir calculation, this difference is felt primarily in the calculated value of total enthalpy in the flow. For the reasons discussed in Section I, it is important to make an accurate assessment of this parameter.

## IV. Calculation of Nozzle Flowfields

Calculation of the steady-state flowfield of the nozzle, with particular interest on the freestream conditions at the front of the model, are currently made using an axisymmetric full Navier-Stokes solver. This calculation has been traditionally made using a quasi one-dimensional algorithm[10]. That type of algorithm includes the treatment of finite rate chemistry recombination, and finite rate vibrational relaxation has been incorporated into it as well. The code typically makes use of the measured Pitot pressure in the freestream at the test station location by altering the geometric area of the nozzle profile to match this given value. This technique provides a simple method to account for the viscous effects of the nozzle without introducing the requirement for a powerful computer. However, this treatment of the problem does not adequately predict the viscous-inviscid interactions in the nozzle, particularly when finite rate chemistry is coupled to these interactions. This technique also does not provide any information about radial gradients in the flowfield. Such flow non-uniformity can be important in comparing computational and experimental data for complex problems[11].

For this reason, two-dimensional calculations are performed for most of the runs in the LENS facilities. Advances in computing power in recent years have made it possible to perform a nozzle calculation of sufficient grid resolution in the same time frame that it takes to perform a run in the facility, so it is now possible for the computation to keep pace with the experiment.

The nozzle code is a full Navier-Stokes solver designed for two-dimensional problems and includes axisymmetric source terms. This code contains several features which have been found to be necessary to successfully solve the nozzle problem. First among these features is the high-pressure correction to the equation of state for non-ideal gas effects in the flow. This correction has already been given in eqn. (8).

The second of these features is the inclusion of proper turbulence modeling for the nozzle. One finds that even for very low density cases in the LENS facilities, the Reynolds number inherent in the nozzle domain are such that some level of turbulent flow is always generated in the throat region of the nozzle, where both density and velocity are sufficiently large. The turbulent boundary layer is distorted as it expands in the divergent section of the nozzle and the density drops rapidly. A typical solution of Reynolds number per unit length versus axial station is shown in Fig. 5. One may see that values exceeding $1x10^9$ per meter occur just downstream of the throat, while the test section Reynolds number has dropped more than three orders of magnitude to approximately $1x10^6$ per meter. Thus, a turbulence model is required that can handle the strong favorable pressure gradient of the flowfield for this application.

So far, two turbulence models have been evaluated for this task. Initially, the Baldwin-Lomax zero equation model was used[12]. This was found to be unable to predict the physics of the strong favorable pressure gradient without user intervention. For this reason, an ad hoc procedure was developed to shut off the turbulence model at an arbitrary location in the nozzle and continue with a laminar solution from there downstream. While this procedure was found to adequately predict the Pitot pressure profiles downstream at the test location, the selection of the re-laminarization location was somewhat arbitrary and difficult to predict. The Spalart-Allmaras one equation turbulence model[13] was next incorporated into the nozzle code with the Catris and Aupiox compressibility correction[14]. With the additional physics afforded by the added equation, the model was found to predict the displacement thickness of the nozzle flow to reasonable accuracy without any adjustable parameters.

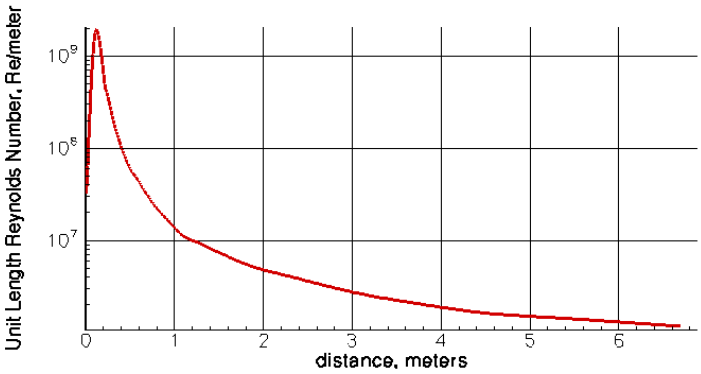


**Figure 5. Centerline Reynolds Number per Unit Length versus Axial Station in a Typical LENS Nozzle Flowfield**

Additionally, non-equilibrium effects must be considered. Although equilibrium was assumed for the reservoir, this will not generally continue to be the case as the flow expands and relaxation times increase. For this reason, finite rate chemistry is employed and the non-equilibrium vibrational energy is treated with a single, lumped vibrational temperature[15]. Vibrational relaxation rates are calculated using the Landau-Tellar model with a Millikan-White rate expression[16]. Because of the large range of length scales, the problem requires very fine grid resolution at the wall, especially in the throat region. The large gradients in the flow combined with the small grid cell size make the problem very numerically stiff. For this reason, the data-parallel line relaxation[17] (DPLR) algorithm is employed by the solver. DPLR provides enhanced stability over many other types of algorithms because of the strong implicit coupling of the large wall-normal gradients of the boundary layer into the Jacobian matrices.

## V. Freestream Flow Condition Calculation Cases

### A. LENS-I D Nozzle with Air Test Gas Calculation

As a first case, we consider a flow in the LENS-I facility using the D nozzle. This nozzle has been used to cover a nominal Mach number range extending from approximately 10 up to 18 using air as a test gas. This first case for consideration is a calibration condition in air using a 2.9 cm (1.125 in) throat size. The run is designated run 188, and was used to calibrate the tunnel in preparation for a high enthalpy code validation exercise for the double cone model. This model is used to generate a laminar shock/separation interaction region over the model. Details and results of this high-enthalpy double cone program are discussed by Holden and Wadhams[18], and computational predictions for this program can be found in Nompelis, et al.[19]. For run 188, the calibration of the facility was made using an array of Pitot pressure probes extending radially out from the nozzle centerline along a ray that was stationed at the test section plane. Later, this same run condition was repeated with the double cone model in place of the Pitot rake assembly.

Using the reservoir calculation method of the previous section, the following values were calculated in the steady-state period of the reservoir at the end of the shocktube: 26.25 MPa (3,806 psia) for stagnation pressure and 6,153 K (11,075 $^{O}$R) for stagnation temperature. A five species air model was used for the reservoir calculation with $N_2$, $O_2$, $NO$, $N$, and $O$ considered as active species. The equilibrium concentrations by mass of these species were found to be 0.702 for $N_2$, 0.036 for $O_2$, 0.113 for $NO$, 0.008 for $N$, and 0.141 for $O$. With these conditions, the total enthalpy of the flow is approximately 10.5 MJ/kg ($1.15 \times 10^8$ ft$^2$/s$^2$).

Several results are shown in Fig. 6. In Fig. 6 (a), contours of Mach number are given, giving a qualitative sense of the expansion process. Here, one may see the growth of the viscous effects on the walls and get a sense of the core flow that is available for testing. In Fig. 6 (b), the contours of the vibrational temperature degree of freedom are given, non-dimensionalized by the local translational temperature. Here, one sees the non-equilibrium expansion of the vibrational temperature, which is in equilibrium with the translational temperature in the reservoir region. As the test gas expands, the vibrational temperature is effectively frozen while the translational temperature continues to decrease. Accurate prediction of this parameter in the freestream flow is important in hypersonic facilities as it affects the distribution of the energy into the internal modes of the gas. It also affects the chemistry recombination rates during the expansion process. In Fig. 6 (c), contours of *NO* are shown, which, like the vibrational temperature, are also effectively frozen in a non-equilibrium state by the nozzle expansion. One may see that while the reservoir contained approximately 11% *NO* by mass, this fraction has been reduced to 3.6% in the freestream. The level of contamination of the test flow by *NO* is an important metric of reflected shock tunnel facilities. This measurement is also difficult to make experimentally, so accurate calculation of the concentration of *NO* in the freestream is a significant contribution to the facility operation through the use of numerical tools. The investigation of the *NO* concentration by experimental measurement is one goal of on-going work by the authors.

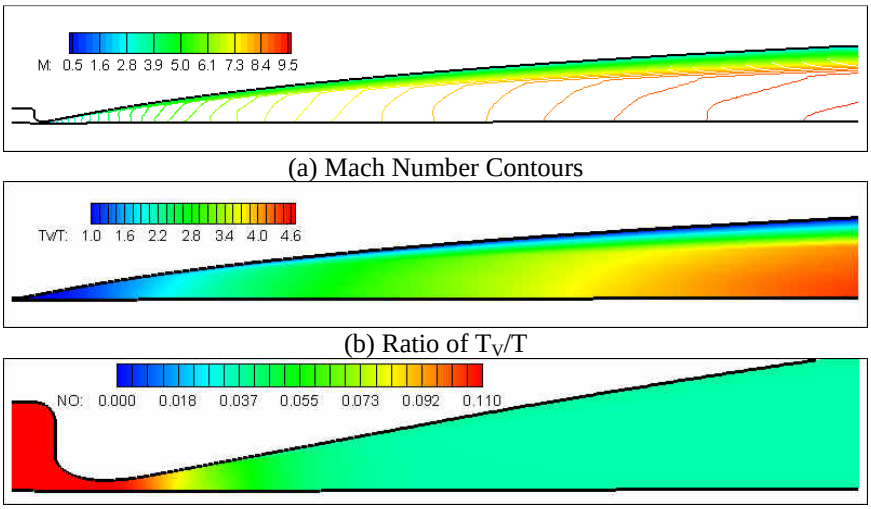


(a) Mach Number Contours

(b) Ratio of $T_V/T$

(c) Mass Fraction, NO

**Figure 6. Relevant Flowfield Features of Solution of LENS-I Run 188 with Air Test Gas**

The accuracy of the nozzle code calculation may be better assessed by direct comparison of the calculated Pitot pressure profile at the test section with the measured values. This comparison is shown in Fig. 7. The measured values are shown, along with values of the data mirrored about the singularity line for better comparison. Across the core region, Fig. 7 shows that both the levels and the trend of the Pitot pressure profile is captured by the calculation. At each Pitot gage location, the computation is within +/-5% or less of the measured value, which is on par with the uncertainty level of the gages overall experimental facility accuracy. The agreement shown in Fig. 7 provides a justification that, despite the thermo-chemical complexities of the high enthalpy flow regime, the calculation is correctly predicting the freestream flow properties.

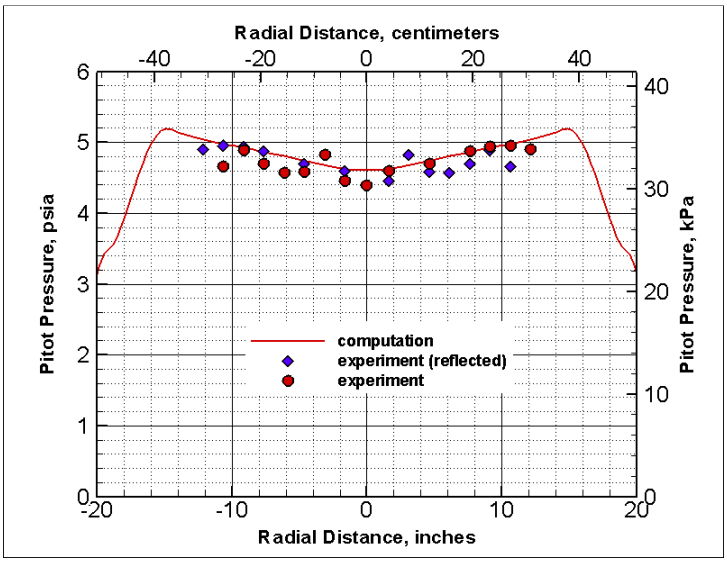


**Figure 7. Comparison of Measured Pitot Pressure with Nozzle Calculation at Test Station with Air Test Gas**

**B. LENS-I D Nozzle with Carbon Dioxide Test Gas Calculation**

The flow of carbon dioxide test gas is also considered in the same LENS-I D nozzle. For this case, designated run 220, the throat size is 4.1 cm (1.6 in). For this case, the reservoir conditions are 96.7 MPa (14,000 psia) reservoir pressure and 3,440 K (6,200 $^{O}$R) reservoir temperature. The total enthalpy of the flow is 5.0 MJ/kg

($5.4x10^7$ $ft^2/s^2$) for this condition. The inclusion of the chemistry and vibrational effects in the nozzle problem is more important for carbon dioxide than for air, as the equilibrium species concentrations of the dissociation reaction for carbon dioxide are quite sensitive to temperature. Also, the characteristic vibrational temperatures of carbon dioxide are much lower than for either molecular nitrogen or molecular oxygen, so a significant amount of the internal energy of carbon dioxide is contained in the vibrational modes even at room temperatures.

Four species were considered for this case: $CO_2$, $CO$, $O_2$, and $O$. Atomic carbon was also initially considered, but this species was found to be unimportant for the range of states over which the LENS-I facility operates. In the reservoir, the equilibrium concentrations of those species were calculated to be 84.1%, 10.1%, 5.6%, and 0.2% respectively by mass. As discussed earlier in Section III, the high density of the gas in the reservoir region of the shock tunnel facility make chemical relaxation times very short when compared to the characteristic run times of the tunnel. Therefore, the equilibrium compositions are the appropriate input values for the nozzle code.

The comparison of the calculation with the measured Pitot pressure profile for run 220 is shown in Fig. 8. Here, one can see the agreement at the centerline, as well as that the calculation has captured the trend of the profile with increasing radius. Both calculation and experiment show that a uniform core exists to at least 41cm (16 in) radius or 82 cm (32 in) diameter. Besides the Pitot pressure comparison, calculation with the nozzle code shows the following resulting centerline values at the test section plane. Test section temperature is 890 K (1,600 $^{O}$R), velocity is 2,845 m/s (9,330 ft/s), pressure is 4,700 Pa (0.68 psia), and Mach number is 6.22. The vibrational temperature was found to equilibrate with the translational temperature throughout the length of the nozzle for this condition because of the relatively high test gas density for which the facility was run. In general, this will not be the case, as significant amounts of vibrational energy may be frozen by the rapid expansion process. Of particular importance is the gas composition, as the amount of carbon monoxide contamination in the test gas flow is essential for evaluating model data in a program. Here, the gas composition was found to be 92.6% carbon dioxide ($CO_2$), 4.7% carbon monoxide (CO), and 2.7% molecular oxygen ($O_2$) by mass. Thus, the LENS-I facility has been used to produce a flow with less than 5% carbon monoxide contamination. The amount of recombination in the non-equilibrium expansion process is an important parameter to look at in making and assessing the calculation of the nozzle flowfield.

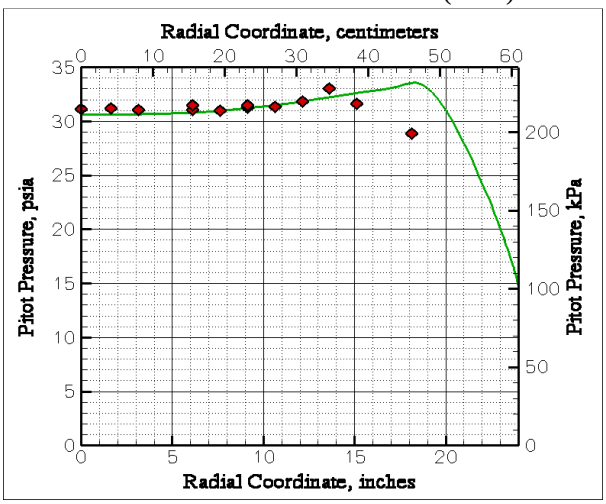


**Figure 8. Comparison of Measured Pitot Pressure (run 220) and Nozzle Calculation at Test Station**

## C. LENS-II M6 Nozzle with Air Test Gas Calculation

Here, we consider a case in the new Mach 6 contoured nozzle for LENS-II. This nozzle was designed by John Korte[20] using the technique of Sivells[21]. As designed, this nozzle has an exit plane diameter of approximately 1.5 m (60 in) and the throat size of this nozzle is 18.3 cm (7.2 in). An alternate throat has also been produced with a size of 12.7 cm (5in) that produces a flow with a nominal Mach number of 7.1. In this case, however, we have considered a case with the original 18.3 cm throat. The case considered, designated run 87, was part of the calibration phase for the aerothermal testing of the Hyfly model[22]. This reservoir pressure is 2.04 MPa (295 psia) and a reservoir temperature of 1,620 K (2,920 $^{O}$R).

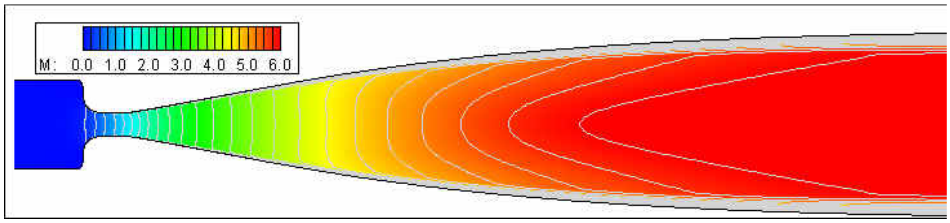


**Figure 9. Mach Number Contours for LENS-II M6 Nozzle Case, Run 87**

The Mach number contour map of the resulting steady-state flowfield is shown in Fig. 9. One should note the exit Mach number of 5.99 at the centerline of the exit plane. Line divisions of Mach number are also shown in Fig. 9 to more clearly illustrate the cancellation of the expansion waves in the diverging section of the nozzle, producing a uniform core in the test section. One may also get a qualitative sense of the boundary layer growth on the nozzle walls from this figure, which is kept to a minimum for this condition. The large core size that is produced can accommodate the full-size Hyfly model. This arrangement with the Hyfly model as located in the nozzle flowfield is shown in Fig. 10. This figure shows contour lines of Mach number with approximately 0.10 incremented divisions. One may notice that the entire model is contained within one single contour division in the flowfield, limiting the total Mach number variation across the model to +/- 0.05, or +/- 1% of the average level. This type of ground test simulation fidelity leads to increased understanding of program design requirements without the need for expensive, high-risk flight tests.

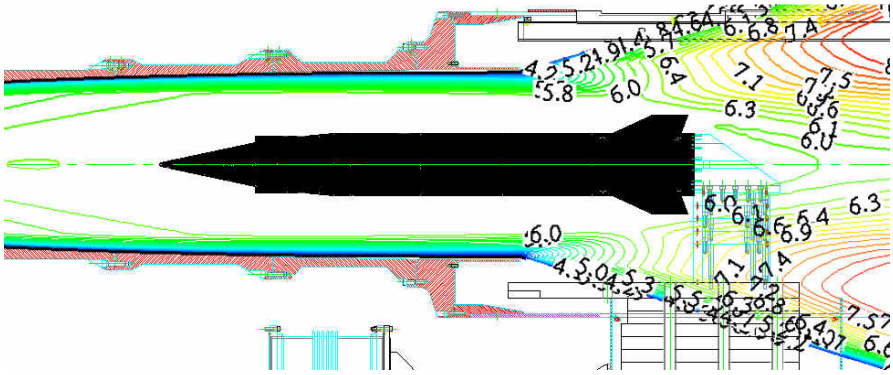

**Figure 10. Placement of Hyfly Model in LENS-II M6 Nozzle Flowfield Test Section**

Further understanding of the exit plane flowfield may be gained by looking at the Pitot pressure profile at this station in Fig. 11. For this station, the measured values are shown as well as those same values mirrored across the singularity line. The computation is also shown for this station. One can see for this case that the nozzle code correctly predicts the measured core flow size of 1.2 m (48 in) as well as the core level of Pitot pressure at all points to +/- 3.5% or less.

The summary plot of the experimental Pitot pressure measurements that were made for all calibration runs in this same series is shown in Fig. 12. Although the computation was only performed for the Run 87 condition, Fig. 12 shows that the same core size of approximately 1.2 m (48 in) is achieved over a range of Reynolds number conditions. The successful design of this newest nozzle for the LENS facilities is demonstrated by the fact that the viscous effects on the nozzle walls are minimal and independent of the freestream flow conditions.

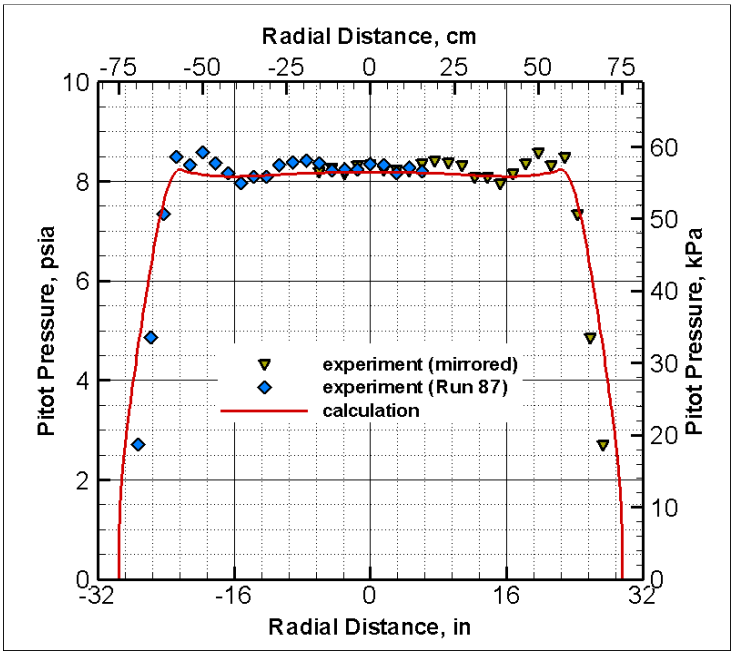


**Figure 11. Pitot Pressure Comparison between Computation and Experiment for LENS-II Run 87 at a Station 55 cm (21.75 in) before (inside) Nozzle Exit Plane**

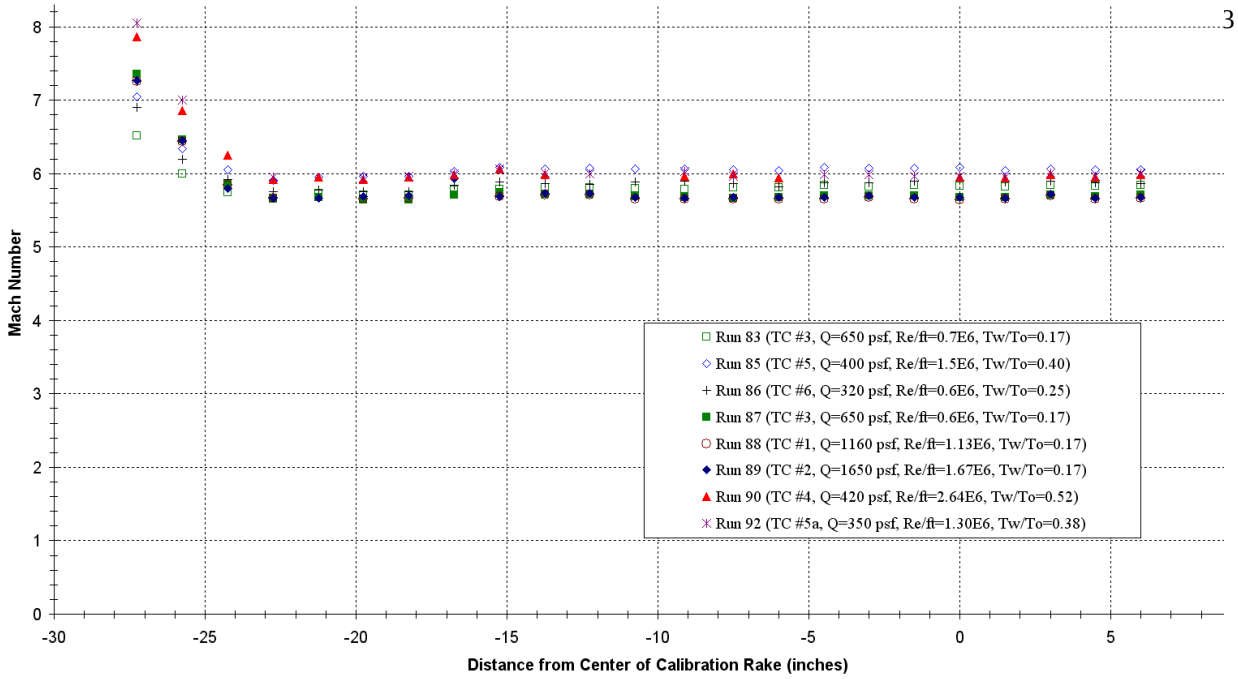


**Figure 12. Comparison of Measured Mach Number Values for Several Test Conditions in the New LENS-II M6 Nozzle**

## VI. Design of Nozzle Throat Inserts for the LENS Facilities using Computation

Although the previous section demonstrated the success of using the Navier-Stokes computations to predict the test section state of the flow for a known nozzle geometry and known set of reservoir conditions, computations of the nozzle flowfield have been used in other ways by CUBRC. One of the problems for which the computation has proven most useful is in the design of new nozzle throat inserts. Each of the nozzles used in the LENS facilities is designed for a particular Mach number with a particular throat size. For instance, in the case of the new LENS-II M6 nozzle, the throat diameter as designed is 18.3 cm (7.2 in) and produces an exit plane flow of approximately Mach 6, as shown from Fig. 12. Ideally, one would create a whole new nozzle with the appropriate area ratio for each new condition one wanted to run. However, such a strategy is obviously not practical. Because of the large size of the LENS facilities, the construction of a new nozzle is a long and costly process. The high cost makes it prohibitive to construct more than a few nozzles for the facilities. Changing from one nozzle to another is also a work-intensive process that can shut the facility down for one to two weeks.

For these reasons, the nozzles in both LENS-I and LENS-II are constructed with removable throat inserts that can be changed for inserts of a different size. The effect of this is to change the geometric (and effective) area ratio of the nozzle to produce a different exit Mach number. Although the change of the throat is not within the design parameter space of the nozzle design process, one finds that, in practice, the nozzle can accommodate a certain amount of increase or decrease in the throat size without unacceptable distortion of the test section flow profile. Usually a change in the throat size tends to reduce the available core size of the test section. This core size continues to shrink as the throat departs farther from the design point until the overall flow quality becomes unacceptable.

The issue that arises in this throat modification process is how to properly contour the throat insert to produce the best possible flowfield in terms of test section quality and uniformity. Although quasi one-dimensional methods have been used to predict the freestream state of the facility, doing so requires a measured test section Pitot pressure in order to compute the nozzle flowfield. This technique also does not provide any two-dimensional sense of how strong the resulting flowfield gradients are. For these two reasons, this type of algorithm is not useful to specify any information about how to re-contour a new throat insert.

As an example of this design process, we consider a recently built throat insert for the M4 nozzle of the LENS-II facility. As designed the M4 nozzle produces a flow of a Mach number of approximately 4.5. As part of NASA return-to-flight program for the space shuttle vehicle, heating levels on the bipod region of the vehicle were measured in the LENS-II facility at the peak loading condition in flight of Mach 4.0. For this program, a new throat was designed for the M4 nozzle to produce the desired condition with a throat minimum diameter of 31.75 cm (12.5 in). At first, this modification was made by creating a new throat insert only and leaving the surrounding endwall and other components as they already existed (for convenience). In this newly created configuration, the existing

endwall contour as connected to the increased size of the new throat insert causes a rapid change in the nozzle contour in the converging section. The sharp angle that the endwall makes with the throat causes a rapid overexpansion, followed by a shock just downstream of the sonic line of the throat. The shock is turned normal to the flow at the centerline by the axisymmetric symmetry boundary condition, and this shock, along with the resulting reflections, are seen in the Schlieren image of Fig. 13. This arrangement causes a significant momentum deficit near the centerline of the flowfield. This deficit is observed even at the exit plane of the nozzle in the test section.

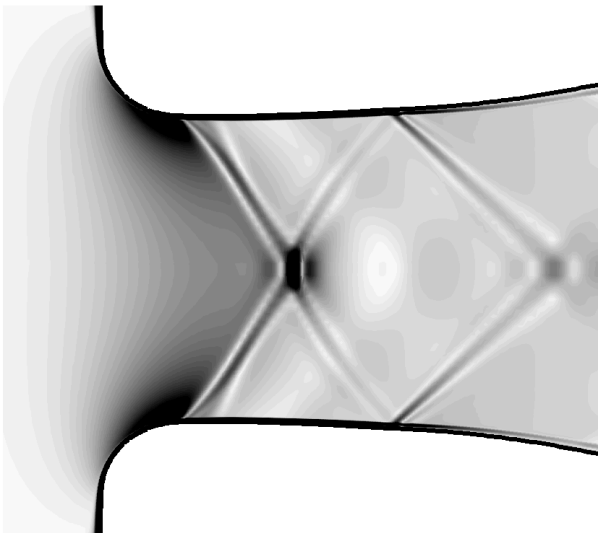

**Figure 13. Computational Schlieren of Nozzle Throat Region Flowfield for Original 31.75 cm (12.5 in) Throat Insert**

In this case, the source of the momentum loss at the centerline of the flowfield was discovered only from the computation. With this understanding, provision to modify the endwall components of the tunnel was made in order to better contour the converging section of the throat. Several different contours were evaluated with the computational code to find the contour which would provide the most uniform flow. As Pitot pressure is a measure of momentum in the flowfield, the measured profiles before and after the endwall alteration are shown in Fig. 14. One sees that the momentum deficit in the center of the flowfield has been eliminated by the geometric change, and that the updated version of the throat assembly provides superior quality flow to the original configuration.

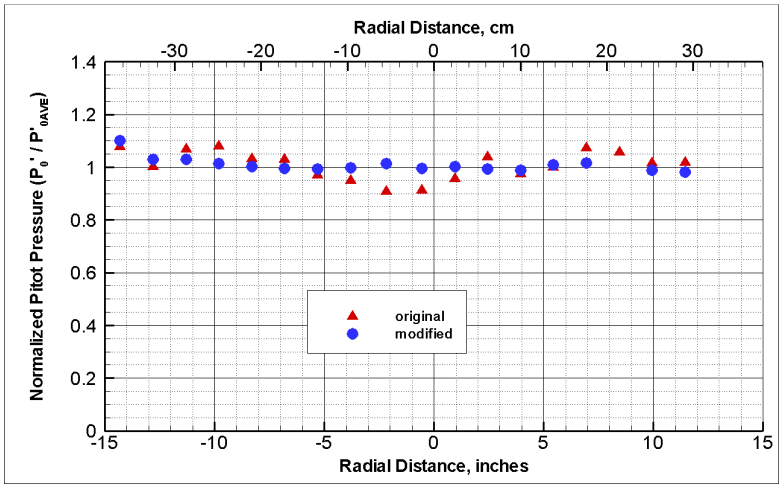


**Figure 14. Comparison of Measured Pitot Pressure Profiles at Test Station of M4 Nozzle with 31.75 cm (12.5 in) Throat Before and After Computation-Driven Contour Modification**

The design of the nozzle throat insert for the LENS facilities is a task that requires the support of numerical Navier-Stokes computations. The example of the M4 nozzle insert for Mach 4 flow has demonstrated that incorrect contouring of the throat component can have destructive effects on the test section flow quality of the facility. Empirical evidence and one-dimensional calculations of the nozzle flowfield do not provide any information about how to correctly contour this throat insert. For this task, the two-dimensional numerical schemes described here have been shown to provide this knowledge.

## VII. Conclusions

We have provided several examples and comparative data sets regarding the integration of Navier-Stokes computational capabilities into the daily operation of the CUBRC LENS shock tunnels. The difficulties encountered in the understanding and assessment of ground test data programs require the use of such numerical algorithms to obtain the accuracy and consistency needed for the design of flight interceptors, high speed engines, and re-entry vehicles.

In computing the nozzle flowfield problem, we have provided a methodology for solving the steady state flowfield in the reservoir and the nozzle. This assumption is justified by the large physical size and the long available run time of the LENS facilities. These features minimize viscous interactions in the shock tube and provide sufficient steady reservoir time that the transient start-up of the nozzle does not occupy a significant portion

of the available test time. The reservoir conditions have been calculated through the assumption of well-tailored shock tube operation. The inclusion of an equation of state for non-ideal gas effects at high pressures can have a significant impact on the computed total enthalpy in the flow. This feature has been shown to be important to the nozzle flowfield calculation because it has an impact on the velocity in the freestream.

The calculation of the nozzle flowfield including chemical and vibrational non-equilibrium effects has been shown to provide agreement with the measured Pitot pressure levels in the test section to an accuracy of +/- 5% or better for each of the cases studied, covering air, nitrogen, and carbon dioxide test gas flows. The addition of this computational capability brings the freestream condition uncertainty to levels on par with other sources of experimental uncertainty in the facilities. Although previous work has shown that one can do almost as well with a simpler, one-dimensional technique, the additional capability to predict both axial and radial gradients in the flow provides deeper understanding of flow interactions with the model.

There are two main uncertainties in making this type of calculation for a reflected shock tunnel facility. The first of these is uncertainty in the determination of the reservoir conditions. As the reservoir conditions are the driving inputs of the nozzle calculation, incorrect reservoir values will, by definition, lead to incorrect freestream values. The second effect is the modeling of turbulence in the throat region of the nozzle. The turbulence model must be able to handle the strong favorable pressure gradient and rapidly decreasing Reynolds number in the expansion process. The viscous effects in the throat region are particularly important because they shape how the sonic line is formed and have been shown to have a strong effect on quality of the test section flowfield in terms of core size and uniformity. Finally, the design procedure for proper throat contouring to control these viscous-inviscid interactions has been shown to benefit strongly by the support of the nozzle calculation.

## Acknowledgments

*CUBRC thanks John Korte for his help in the successful design of the M6 contoured nozzle for the LENS-II facility.*

*Portions of this work were sponsored by the Air Force Office of Scientific Research under grant FA9550-04-1-0341. The views and conclusions contained herein are those of the authors and should not be interpreted as necessarily representing the official policies or endorsements, either expressed or implied, of the AFOSR or the U.S.~Government.*

## References

[1]Anderson, John. *Modern Compressible Flow*. 2ND Ed. McGraw-Hill: Boston, Mass, 1990.

[2]Lu, F.K. and Marren, D.E. Eds. *Advanced Hypersonic Test Facilities*. AIAA Progress in Astronautics and Aeronautics Series: Vol 198. Chapter 4. Reston, VA: American Institute of Aeronautics and Astronautics, 2002.

[3]Nompelis, I.; Candler, G.V.; Wadhams, T.P.; and Holden, M.S. "Numerical Simulation of High-Enthalpy Experiments in the LENS-X Expansion Tube Facility". AIAA 2004-1000. 42ND Aerospace Sciences Meeting & Exhibit. Reno, NV: 5-8 Jan, 2004.

[4]Holden, M.; Maclean, M.; Wadhams, T.; and Walker, B. "Development & Application of New Ground Tests Capability to Conduct Full-Scale Shroud/Stage Separation". AIAA 2005-0696. 43RD Aerospace Sciences Meeting & Exhibit. Reno, NV: 10-14 Jan, 2005.

[5]Holden, M.S. and Wadhams, T.P. "A Database of Aerothermal Measurements in Hypersonic Flows in 'Building Block' Experiments for CFD Validation". AIAA 2003-1137. 41ST Aerospace Sciences Meeting & Exhibit. Reno, NV: 4-7 Jan, 2003.

[6]Holden, M.S., Wadhams, T.P., Harvey, J.K. "Comparisons Between DSMC and Navier-Stokes Solutions on Measurements in Regions of laminar Shock Wave Boundary Layer Interaction in Hypersonic Flows". AIAA 2002-0435. 40TH Aerospace Sciences Meeting & Exhibit. Reno, NV: 14-17 Jan, 2002.

[7]Gaydon, A.G. and Hurle, I.R. *The Shock Tube in High-Temperature Chemical Physics*. New York: Reinhold Publishing Co., 1963.

[8]Lordi, J.A. and Mates, R.E. *Non-equilibrium Expansions of High-Enthalpy Airflows*. Cornell Aeronautical Laboratory Report, ARL 64-206. November 1964.

[9]McBride, B.; Zehe, M.; and Gordon, S. *NASA Glenn Coefficients for Calculating Thermodynamic Properties of Individual Species*. NASA/TP-2002-211556. September 2002.

[10]Lordi, J.A.; Mates,R.E.; and Moselle,J.R. *Computer Program for the Numerical Solution of Nonequilibrium Expansions of Reacting Gas Mixtures*. Cornell Aeronautical Laboratory (CAL) Report, AD-1689-A-6. October, 1965.

[11]Nompelis, I.; Candler, G.; and Holden, M. "Effect of Vibrational Nonequilibrium on Hypersonic Double-Cone Experiments". *AIAA Journal*. Vol 41, no 11. Pgs. 2162 – 2169. November 2003.

[12]Baldwin, B.S. and Lomax, H. "Thin Layer Approximation and Algebraic Model for Separated Turbulent Flows". AIAA Paper 78-0257. Huntsville, AL: 1978.

[13]Spalart, P.R. and Allmaras S.R. "A One-Equation Turbulence Model for Aerodynamic Flows". AIAA 92-0439. 30TH Aerospace Sciences Meeting & Exhibit. Reno, NV: 6-9 Jan, 1992.

[14]Catris S. and Aupoix B. "Improved Turbulence Models for Compressible Boundary Layers." AIAA 98-2696. 2ND Theoretical Fluid Mechanics Meeting: Albuquerque, NM, June 1998.

[15]Candler, G.V. "Chemistry of External Flows". *Aerothermochemistry for Hypersonic Technology*: Von Karman Institute for Fluid Dynamics Lecture Series. VKI LS 1995-04.

[16]Millikan, R.C. and White, D.R. "Systematics of Vibrational Relaxation". J. Chem. Phys., Vol 39, Pgs. 3209-3213. 1963.

[17]Wright, M.J.; Bose, D.; and Candler, G.V. "A Data Parallel Line Relaxation Method for the Navier-Stokes Equations". *AIAA Journal*. Vol 36, no 9. Pgs 1603 – 1609. Sept 1998.

[18]Holden, M.S. and Wadhams, T.P. "A Review of Experimental Studies for DSMC and Navier-Stokes Code Validation in Laminar Regions of Shock/Shock and Shock/Boundary Layer Interaction Including Real Gas Effects in Hypervelocity Flows". AIAA 2003-3641. 2003.

[19]Nompelis, I.; Candler, G.; Holden, M.; and Wadhams, T. "Numerical Investigation of High Enthalpy Chemistry on Hypersonic Double-Cone Experiments". AIAA 2005-0584. 43RD Aerospace Sciences Meeting & Exhibit. Reno, NV: 10-14 Jan, 2005.

[20]Chadwick, K.M.; Holden, M.S.; Korte, J.J.; and Anderson, E.C. "Design and Fabrication of a Mach 8 Contoured Nozzle for the LENS Facility". AIAA Paper 96-0585. 34TH Aerospace Sciences Meeting and Exhibit. Reno, NV: 15-18 Jan, 1996.

[21]Sivells, J.C. "Aerodynamic Design of Axisymmetric Hypoersonic Wind-Tunnel Nozzles". *Journal of Spacecraft and Rockets*. Vol 7, no 11. Pgs 1292 – 1299. November 1970.

[22]Hyfly Program website. <*http://www.darpa.mil/tto/programs/hyfly.html*>. Accessed 1 January 2005.